Available online at www.sciencedirect.com
ScienceDirect
International Journal of Thermal Sciences 46 (2007) 1275–1284
International Journal of Thermal Sciences
www.elsevier.com/locate/ijts

A numerical study on developing laminar forced convection and entropy generation in half- and double-sine ducts

T.H. Ko *

Department of Mechanical Engineering, Lunghwa University of Science and Technology, 300, Wan-Shou Rd. Sec. 1, Kueishan, 33306 Taoyuan, Taiwan

Received 30 January 2006; received in revised form 4 January 2007; accepted 4 January 2007

Available online 20 February 2007

Abstract

In the present paper, the developing laminar forced convection and entropy generation in both double- and half-sine ducts are investigated with numerical methods. The studied cases cover *Re* ranging from 86 to 2000. The duct aspect ratio (Λ/a) and the external heat flux (q^*) are varied as $\Lambda/a = 2$, 4 and 8, and the values of q^* are varied as 0.0405, 0.0811 and 0.1622, respectively. The comparisons of the flow features, including the distributions of axial velocity, temperature, Nusselt number and the local entropy generation, in the double- and half-sine ducts are provided in detail in the paper. Particularly, the optimal analysis of the two-type ducts based on the minimal entropy generation principle is the major concern. Through the evaluations of the overall entropy generation in the whole flow domain, the optimal option between the double- and half-sine duct is found to be dependent on the duct aspect-ratio, external heat flux and *Re*. Among all the cases studied, the half-sine duct with $\Lambda/a = 2$ is found to have the minimal entropy generation, and therefore is concluded as the optimal option for achieving the least irreversibility and best exergy utilization in the thermal system.

Keywords: Entropy generation; Double-sine duct; Half-sine duct; Aspect ratio; Minimal entropy generation principle; Irreversibility; Exergy

1. Introduction

Heat exchange passages with chevron-wave surface are widely employed in plate heat exchangers. The corrugations along the length of passage periodically disrupt the flow and in turn significantly enhance the heat transfer performance. Fig. 1 shows the configuration of a plate heat exchanger with corrugations of the sinusoidal profile. The relevant studies on the heat transfer and fluid dynamics in chevron-type plate heat exchangers are abundant, e.g. the good review work by Shah and Focke [1], the systematical analysis of the effect of the corrugation inclination angle on the thermal-hydraulic performance of the heat exchanger by Focke et al. [2] and Heavner et al. [3], the useful correlations of friction factors and heat-transfer coefficient for plate heat exchangers as functions of the corrugation inclination angle and Reynolds number provided by Martin [4], and the numerical analysis of the three-dimensional heat transfer and fluid flow in chevron plate channels by Jang and Lin [5]. When corrugations of the two plates are phase shifted by π, and the chevron inclination angle β is zero (see Fig. 1), the flow configuration becomes a limiting case with straight longitudinal flows in a number of parallel channels with a sinusoidal-shape cross-section. Because of practical importance, the relevant studies on the limiting case have been carried out by many researchers [6–8]. Fisher and Martin [6] analyzed the friction factors for fully developed laminar flow in ducts confined by corrugated parallel walls with numerical methods. In the works of Ding and Manglik [7] and Manglik and Ding [8], the analytical solutions of two-dimensional laminar, fully developed flows in double-sine ducts were reported by using the Galerkin function-based integral method.

In the recent design work of a thermal system, the efficient utilization of exergy has been treated as an essential consideration except the analysis from the view point of Thermodynamic First Law. In the contemporary trend, irreversibility and entropy generation in the flow field have been adopted as a gauge for evaluating the optimization of a thermal system. Based on the minimal entropy generation principle [9,10], considerable opti-

* Tel.: +886 2 82093211; fax: +886 2 82091475.
E-mail address: thko@mail.lhu.edu.tw.

1290-0729/$ – see front matter
doi:10.1016/j.ijthermalsci.2007.01.014

Nomenclature

a	half amplitude of the sinusoidal corrugation	mm	
Be	Bejan number		
d_h	hydraulic diameter		
f	friction factor		
$\overline{h}$	average heat transfer coefficient in the duct		
k	thermal conductivity	W/m-K	
K	friction factor, $K = fRe$		
L	distance between the centers of the upper and lower port holes of the chevron plate		
Nu	average Nusselt number		
p	pressure	Kpa	
q''	wall heat flux	W/m^2	
q^*	non-dimensional wall heat flux, $q^* = q''a/kT_0$		
$\dot{Q}$	heat transfer rate	W	
Re	Reynolds number		
S'''_P	volumetric entropy generation rate due to friction	W/m^3-K	
S'''_T	volumetric entropy generation rate due to heat transfer	W/m^3-K	
S'''_{gen}	total volumetric entropy generation rate due to heat transfer	W/m^3-K	
S^*_P	non-dimensional entropy generation rate due to friction		
S^*_T	non-dimensional entropy generation rate due to heat transfer		
S^*_{gen}	non-dimensional entropy generation rate		
T	temperature	K	
T_0	temperature at axial entrance	K	
T_b	bulk mean temperature on a $z =$ constant cross-sectional plane	K	
T_W	wall temperature	K	
T^*	non-dimensional temperature, $T^* = (T - T_0)/T_0$		
V_1	volume of duct	m^3	
W	axial velocity	m/s	
W_0	axial velocity at duct entrance	m/s	
W^*	non-dimensional axial velocity, $W^* = W/W_0$		
$\overline{W}$	average velocity in duct	m/s	
Φ	the area enlargement factor		
Λ	wavelength of the sinusoidal corrugation	mm	
μ	molecular viscosity	kg/m-s	
β	chevron inclination angle		
ρ	density	kg/m^3	

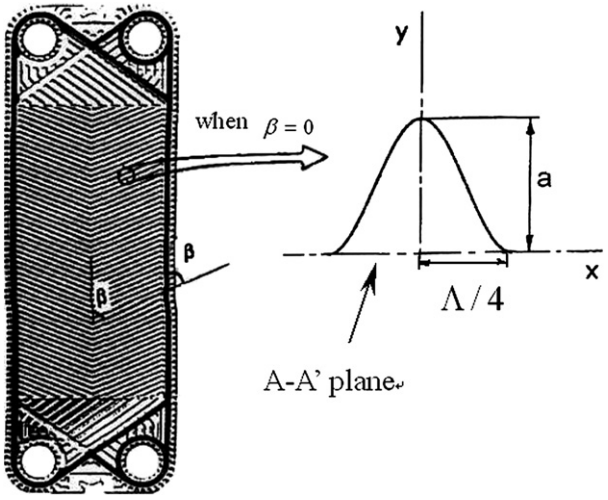

Fig. 1. Configurations of a typical chevron plate heat exchanger and coordinate system of double- and half-sine ducts. A–A′ plane: symmetric plane for double-sine duct; plate wall for half-sine duct.

mal designs of thermal systems have been proposed [11–20]. However, as for the chevron-type heat exchangers, most of the past researches were restricted to the Thermodynamic First Law. The relevant exergy analysis is still very rare. Recently, Ko [21] presented a study focusing on the entropy generation and developing laminar forced convection in a double-sine duct with a fixed aspect ratio. The study adopted both of the theoretically thermodynamic and numerical analyses, and the optimal Reynolds number for the developing laminar forced convection were reported based on minimal entropy generation principle. Later, Ko [22] investigated the entropy generation in a double-sine duct with various aspect ratio, Reynolds number, and wall heat flux by numerical methods. The optimal Reynolds number and optimum aspect ratio were emphasized in the study.

In practical applications, the half-sine duct is also an important option as well as the double-sine configuration. Nonetheless, the studies focusing on the half-sine duct are relatively rare in previous publications. For providing the detailed flow information, including heat transfer performance, friction factor and especially the exergy utilization in the flow fields of the two different-type ducts, the present paper intends to analyze the developing laminar forced convection and entropy generation in both double- and half-sine ducts. Through the results, the competition between the two flow configurations will be evaluated based on the minimal entropy generation principle.

2. Configuration and parameters of a chevron plate heat exchanger

Figs. 1 and 2 show the flow cross-sectional geometry and coordinate system for the sinusoidal-shape duct in a typical chevron plate passages ($\beta = 0°$). In the figure, A–A′ plane represents a symmetric plane for double-sine ducts, whereas it represents a plate wall for the half-sine ducts. The amplitude of the sinusoidal corrugation and wavelength are $2a$ and Λ, respectively. The duct length is L. The characteristic length for the present problem is the hydraulic diameter, d_h, which is defined as four times of fluid volume divided by surface area, and can be calculated as:

$$d_h = 4A/P_w$$

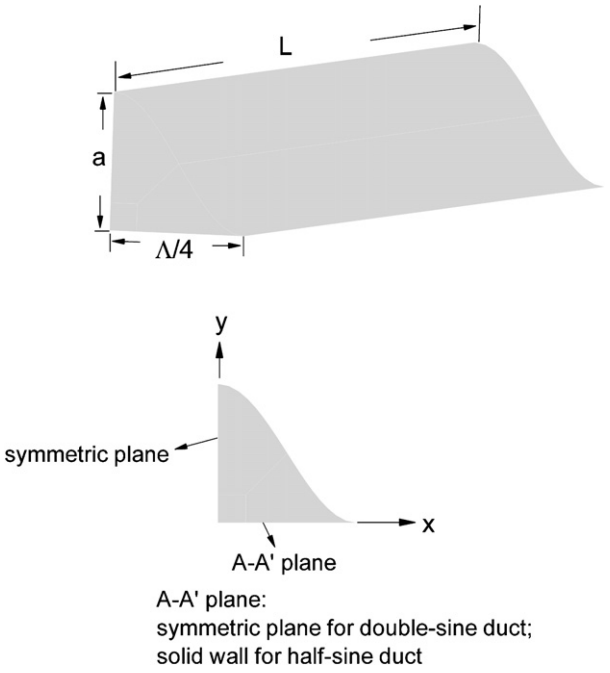

Fig. 2. The analyzed flow passage of the sinusoidal-shape duct (the boundary lines shown within the duct indicate the computational sub-domains).

where A and P_w are the flow cross-sectional area and wetted perimeter, respectively. Reynolds number (Re) and Nusselt number (Nu), are defined as follows:

$$Re = \rho \overline{W} d_h/\mu, \qquad Nu = \bar{h} d_h/k$$

where $\overline{W}$ and $\bar{h}$ are the average velocity and average heat transfer coefficient in the chevron plate. The working fluid in current studies is air. Due to the small temperature change in the flow field, the thermophysical properties of molecular viscosity (μ), thermal conductivity (k) and density (ρ) are assumed to be constants as 1.846×10^{-5} kg/m-s, 0.0263 W/m-K and 1.161 kg/m^3, respectively. The Reynolds number at duct entrance covers ranges from 86 to 2000. The non-dimensional wall heat flux, q^*, is defined according to the external wall heat flux, q'', as $q^* = q'' a/kT_0$, where T_0 is the inlet fluid temperature. The values of q^* are varied as 0.0405, 0.0811 and 0.1622. Three aspect-ratio cases, including $\Lambda/a = 2$, 4 and 8, are investigated. For all the calculated cases, L is fixed as 100 mm. According to the different values of d_h in various Λ/a cases, the minimal L/d_h among all calculated cases is larger than 28. This duct length is assumed to be long enough for the flow to assume fully developed, or at least approximately fully developed, conditions in most cases of the current study.

3. Mathematical model and numerical methods

3.1. Mathematical model

The developing flow as well as fully developed flow region is included in the present problem. The flow is assumed as three-dimensional, laminar, incompressible and steady. The continuity equation, Navier–Stokes equation and energy equation are solved simultaneously. These equations in tensor form are as follows:

$$\frac{\partial U_i}{\partial x_i} = 0 \tag{1}$$

$$\frac{\partial}{\partial x_j}(\rho U_i U_j) = -\frac{\partial P}{\partial x_j} + \frac{\partial}{\partial x_j}\left[\mu\left(\frac{\partial U_i}{\partial x_j} + \frac{\partial U_j}{\partial x_i}\right)\right] \tag{2}$$

$$\frac{\partial}{\partial x_j}\left(\rho U_j C_p T - k\frac{\partial T}{\partial x_j}\right) = U_j \frac{\partial P}{\partial x_j} + \mu\left(\frac{\partial U_i}{\partial x_j} + \frac{\partial U_j}{\partial x_i}\right)\frac{\partial U_i}{\partial x_j} \tag{3}$$

Because of the symmetric configuration, only 1/4 part of the double-sine duct and 1/2 part of the half-sine duct are calculated, respectively. The boundary conditions are as follows.

For double-sine ducts:

(1) on symmetric planes: symmetric conditions are applied for all variables;
   - on $x = 0$ plane: $\partial V/\partial x = \partial W/\partial x = \partial T/\partial x$, $U = 0$;
   - on $y = 0$ plane: $\partial U/\partial y = \partial W/\partial y = \partial T/\partial y$, $V = 0$;

(2) at duct inlet: $U = V = 0$, $W = W_0$ (inlet axial velocity), $T = T_0$ (inlet fluid temperature);
(3) at outlet: $\partial U/\partial z = \partial V/\partial z = \partial W/\partial z = \partial T/\partial z = 0$;
(4) on duct walls: $U = V = W = 0$, $q'' = q_W$.

For half-sine ducts:

(1) on symmetric plane ($x = 0$ plane): symmetric conditions are applied for all variables; $\partial V/\partial x = \partial W/\partial x = \partial T/\partial x$, $U = 0$;
(2) at duct inlet: $U = V = 0$, $W = W_0$, $T = T_0$;
(3) at outlet: $\partial U/\partial z = \partial V/\partial z = \partial W/\partial z = \partial T/\partial z = 0$;
(4) on duct walls and $y = 0$ plane wall: $U = V = W = 0$, $q'' = q_W$.

As the velocity and temperature distributions of the flow field are solved, the friction factor, f, and Nusselt number, Nu, can be calculated as follows.

$$f = \frac{1}{2}\frac{d_h}{\rho \overline{W}^2}\left(-\frac{dP}{dz}\right) \tag{4}$$

Local Nusselt number at a z = constant position:

$$Nu = q'' d_h/k(T_W - T_b) \tag{5}$$

where T_W and T_b are the average wall temperature and bulk mean temperature on a cross-sectional plane at a specific z position:

$$T_b = \frac{1}{\overline{W} A}\int_A W T \, dA \tag{6}$$

In addition, the volumetric entropy generation due to the heat transfer (S'''_T) and friction (S'''_P) can be calculated by the following equations [10]:

$$S'''_T = \frac{k}{T^2}\left(|\nabla T|\right)^2 \tag{7}$$

$$S'''_P = \frac{\mu}{T}\left(\frac{\partial U_i}{\partial x_j} + \frac{\partial U_j}{\partial x_i}\right)\frac{\partial U_i}{\partial x_j} \tag{8}$$

The total volumetric entropy generation in the flow field can be obtained by

$$S'''_{\text{gen}} = S'''_T + S'''_P \tag{9}$$

3.2. Numerical method

The unstructured grid system is used for the present computations. All the above-mentioned equations accompanied with boundary conditions are discretized by a finite volume formulation. In the equations, the convective terms are modeled by the second-order upwind scheme; meanwhile the diffusive terms are modeled by the central difference scheme. The well-known semi-implicit SIMPLE algorithm developed by Launder and Spalding [23] is adopted as the numerical solution procedure. All the detailed numerical procedures are given in [24]. The convergent criteria is set as the relative residual of all variables, including mass, all velocity components and temperature less than 10^{-5}. The CFD software CFD RC (ESI US R&D, Inc.) [25] is used for the numerical solutions.

4. Results and discussion

4.1. Grid independent test and code validation

The grid independent test has been carried out in the previous work of Ko [22]. In the study, three grid systems, including 33 417, 59 697 and 119 997 grid points, are adopted to calculate the flows in a double-sine duct with $\Lambda/a = 4$. The grid system with 59 697 grid points is concluded as dense enough to get the grid independent solutions. Accordingly, the grid system with 59 697 grid points is used.

The accuracy validation of the present numerical solutions has been checked through the computation of flow fields in double-sine ducts as well as in half-sine ducts. For double-sine ducts, the numerical predictions of friction factor and Nusselt number under fully developed condition have been compared with the analytical solutions based on the Galerkin integral method presented by Manglik and Ding [8]. The comparisons cover three aspect-ratio cases of $\Lambda/a = 2, 4$ and 8, and were shown in Table 1, from which the numerical solutions can be seen to have reasonable accuracy. The verification of the numerical accuracy for half-sine duct cases is further performed in the present study. The friction factors for the half-sine ducts of the cases with aspect ratio equal to 2, 4 and 8 were compared with those obtained by Fisher and Martin [6]. The results of accuracy validation are shown in Table 2, from which the present numerical solutions exhibit good predictive accuracy.

Table 1
Comparison of friction factors and Nusselt numbers of double-sine ducts with Ref. [8]

Λ/a	Present solution		Ref. [8]	
	K	Nu	K	Nu
2	14.91	3.09	14.86	3.32
4	13.36	3.31	13.35	3.32
8	11.41	2.55	11.44	2.72

Table 2
Comparison of friction factors of half-sine ducts with Ref. [6]

Λ/a	K [present solution]	K [6]
2	51.91	52.04
4	44.46	44.73
8	40.54	40.56

4.2. Comparison of flow fields in double- and half-sine ducts with $\Lambda/a = 4$, $q^* = 0.0811$ and $Re = 550$

The baseline cases with $\Lambda/a = 4$, $Re = 550$ and $q^* = 0.0811$ of double- and half-sine ducts are discussed first. Figs. 3(a) and (b) show the non-dimensional axial velocity (W^*, defined as W/W_0, is shown in upper row) and temperature (T^*, defined as $(T - T_0)/T_0$, is shown in lower row) contours on the cross-sectional planes at $z/a = 5$, 10, 15, 20 and 40 for double- and half-sine ducts, respectively. Due to the wall effects and boundary layer development, it can be seen that the higher-velocity fluids distribute in the duct central core with increasing area and magnitudes of largest velocity along the downstream for both cases. The largest W^* in half-sine duct is 2.0, which is larger than 1.71 in double-sine duct. The result comes from that the flow space is narrower in half-sine ducts and therefore acuter acceleration is induced. From the distributions of temperature T^*, it can be seen the temperature rise is more important in the half-sine duct, in which the maximum T^* is 0.15 and appears in the sharp lower corner. The maximum T^* in the double-sine duct appears in the top and lower corners, and its value is only 0.08, nearly half of the maximum T^* in the half-sine duct. The higher T^* in the corner region indicates the heat transfer performance is poor in the region. Fig. 4 shows the axial distributions of Nu along duct axis for double- and half-sine ducts, respectively. In both cases, Nu gradually decreases from the highest value at duct entrance toward the fully developed values as flow develops along the downstream. The theoretical value of fully developed Nu for double-sine ducts with $\Lambda/a = 4$ reported by Manglik and Ding [8] is 3.32. Clearly, the value of Nu along the axial duct obtained by the current calculation of double-sine duct as shown in Fig. 4 asymptotically approaches to the theoretical fully developed value. In addition, due to the more effective convection in the wider flow space in double-sine ducts, Nu is seen to have higher values in double-sine ducts.

4.3. Comparison of distributions of entropy generation in double- and half-sine ducts with $\Lambda/a = 4$, $q^* = 0.0811$ and $Re = 550$

Figs. 5(a) and (b) provide the local distributions of Be (upper row in the figure) and entropy generation, S'''_{gen} (lower row in the figure), in double- and half-sine ducts, on cross-sectional planes at $z/a = 5$, 10, 15, 20 and 40 for $\Lambda/a = 4$ case with

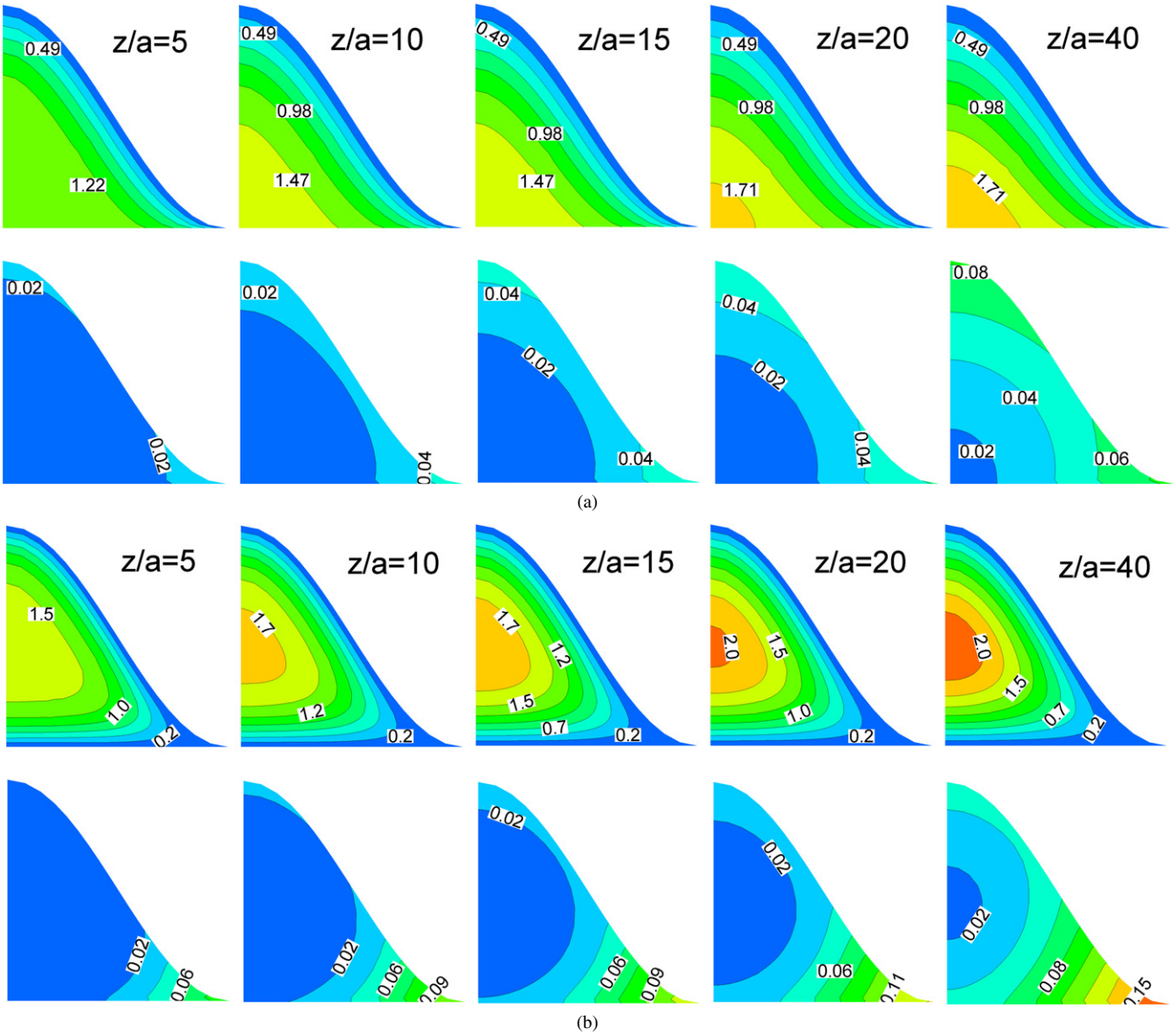

Fig. 3. (a) Contours of non-dimensional axial velocity (W^*) (upper row) and temperature (T^*) (lower row) on cross-sectional planes at $z/a = 5$, 10, 15, 20 and 40 for double-sine duct. $\Lambda/a = 4$, $q^* = 0.0811$, $Re = 550$. (b) Contours of non-dimensional axial velocity (W^*) (upper row) and temperature (T^*) (lower row) on cross-sectional planes at $z/a = 5$, 10, 15, 20 and 40 for half-sine duct. $\Lambda/a = 4$, $q^* = 0.0811$, $Re = 550$.

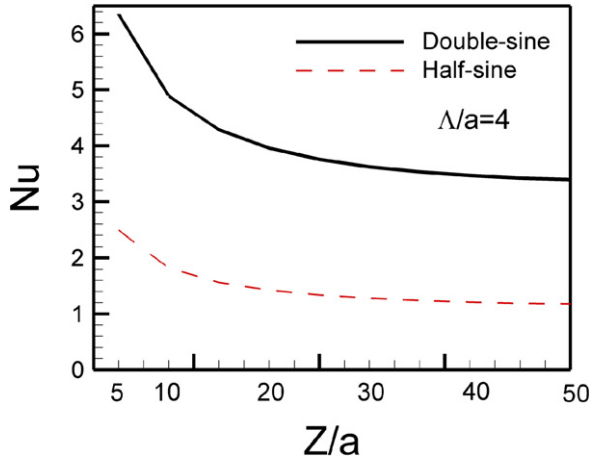

Fig. 4. Axial distributions of Nu for double- and half-sine ducts. $\Lambda/a = 4$, $q^* = 0.0811$, $Re = 550$.

$q^* = 0.0811$, $Re = 550$, respectively. The figures clearly indicate S'''_{gen} in the half-sine duct is larger than that in the double-sine duct. In both cases, S'''_{gen} in the duct central core is minor, whereas the most serious entropy generation concentrates in the duct right-lower corner, which results from the important velocity and temperature gradients in the region. The largest S'''_{gen} in half-sine duct (267 W/m^3-K) is much larger than the largest value (100 W/m^3-K) in double-sine duct. From the distributions of Be, the entropy generation in both cases under the current flow conditions can be judged as dominated by heat transfer irreversibility since Be on all planes in both cases is larger than 0.5. Notably, the values of Be in the double-sine duct are generally larger than those in half-sine duct, which indicates the entropy generation is dominated by heat transfer irreversibility in double-sine duct.

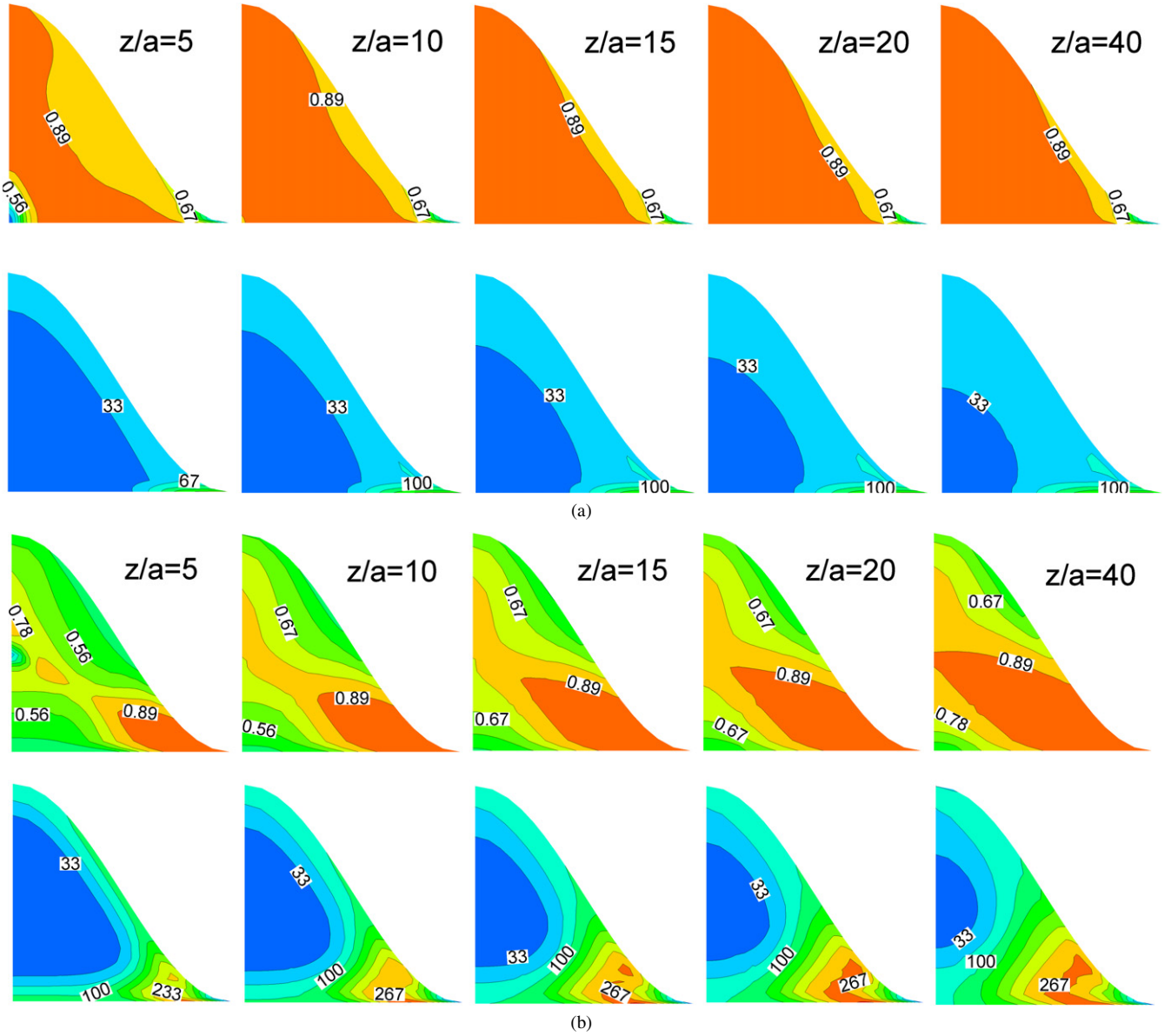

Fig. 5. (a) Contours of Be (upper row) and entropy generation, S'''_{gen} (lower row) on cross-sectional planes at $z/a = 5$, 10, 15, 20 and 40 for double-sine duct. $\Lambda/a = 4$, $q^* = 0.0811$, $Re = 550$. (b) Contours of Be (upper row) and entropy generation, S'''_{gen} (lower row) on cross-sectional planes at $z/a = 5$, 10, 15, 20 and 40 for half-sine duct. $\Lambda/a = 4$, $q^* = 0.0811$, $Re = 550$.

4.4. Comparison of the effects of Re on entropy generation in double- and half-sine ducts for $\Lambda/a = 4$ and $q^* = 0.0811$

In the following, the non-dimensional entropy generation rate, S_P^*, S_T^* and S_{gen}^*, in whole chevron channel are defined by

$$S_P^* = \frac{\int_{V_1} S_P''' \, dV}{\dot{Q}/T_0}, \quad S_T^* = \frac{\int_{V_1} S_T''' \, dV}{\dot{Q}/T_0} \quad \text{and} \quad S_{\text{gen}}^* = \frac{\int_{V_1} S_{\text{gen}}''' \, dV}{\dot{Q}/T_0} \tag{10}$$

where V_1 is the total volume of the duct. It is noted that V_1 for the double-sine duct is twice that of the half-sine duct due to the larger flow space. For detecting the influences of Re on the entropy generation in the flow fields, the cases with Re in range of 86 to 2000 are investigated. Fig. 6 shows the influences of Re on the entropy generation due to heat transfer irreversibility (S_T^*) and fluid friction irreversibility (S_P^*) for double- and half-sine ducts with $\Lambda/a = 4$ and $q^* = 0.0811$. In both the double- and half-sine cases, the increase of Re causes the increase of S_P^* and decrease of S_T^* simultaneously. When Re is low (Re less than 1457 in double-sine duct or less than 1054 in half-sine duct), S_T^* is larger than S_P^*, and vice versa as Re becomes high. The results come from the effects of Re that the higher-Re induces more serious velocity gradients, and thus produces larger S_P^*. Meanwhile, as Re increases, the heat transfer is enhanced, and therefore the temperature gradients and S_T^* are reduced. The conflict influence of Re on S_P^* and S_T^* produces the optimization problem. Under the current flow configuration and heat flux, it can be seen for all Re cases S_P^* is smaller in double-sine ducts,

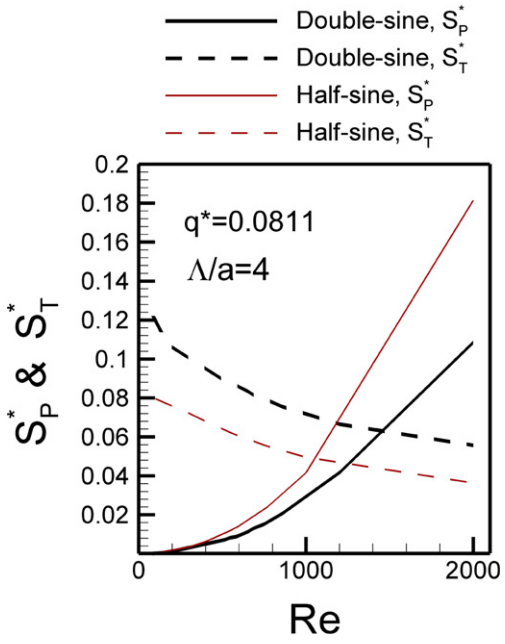

Fig. 6. Effects of Re on S_T^* and S_P^* for double- and half-sine ducts. $\Lambda/a = 4$, $q^* = 0.0811$.

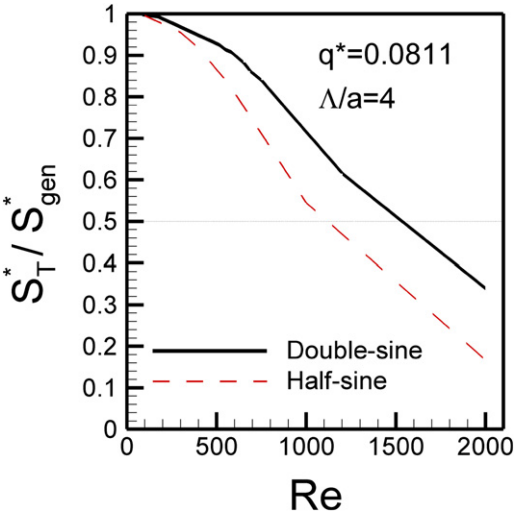

Fig. 7. Effects of Re on S_T^*/S_{gen}^* for double- and half-sine ducts. $\Lambda/a = 4$, $q^* = 0.0811$.

and S_T^* is smaller in half-sine ducts. As Re increases, the difference between the magnitudes of S_P^* in the two-type ducts increases, whereas the difference between the magnitudes of S_T^* decreases. The results exhibit that the more serious frictional irreversibility occurs in half-sine duct as Re increases, but the increase of Re reduces the difference of heat transfer irreversibility between double- and half-sine ducts. Fig. 7 shows the effects of Re on S_T^*/S_{gen}^* for the two-type ducts. It can be seen the values of S_T^*/S_{gen}^* decrease as Re increases, which verifies again the increase of Re causes the increase of S_P^* and the decrease of S_T^*, and accordingly the entropy generation is more dominated by S_P^* rather than S_T^* in the higher-Re cases. Notably, S_T^*/S_{gen}^* is smaller in half-sine ducts for all Re cases, which indicates the flows in half-sine duct sustain more

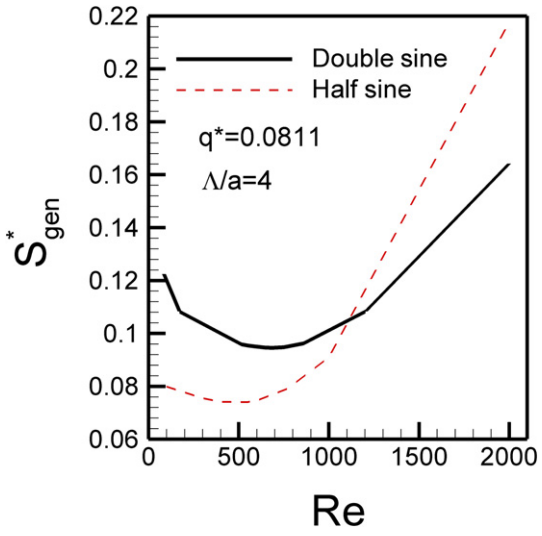

Fig. 8. Effects of Re on S_{gen}^* for double- and half-sine ducts. $\Lambda/a = 4$, $q^* = 0.0811$.

frictional irreversibility than heat transfer irreversibility. The influence of Re on the resultant entropy generation is shown in Fig. 8. Clearly, the optimal Re, with which the S_{gen}^* is minimum, exists in both-type ducts. The optimal Re for double- and half-sine ducts is 550 and 680, respectively, under the current flow conditions. Besides, it can be found the two lines in Fig. 8 intersect at $Re = 1125$. When Re is less than 1125, S_{gen}^* in the half-sine duct is lower than that in the double-sine duct, and accordingly half-sine duct is judged as the favorable choice. On the contrary, the favorable choice turns to be the double-sine duct when Re is larger than 1125.

4.5. Comparison of effects of aspect ratio and heat flux on S_{gen}^* in double- and half-sine ducts

Fig. 9 shows the relationship between S_{gen}^* and Re for the two-type ducts with $q^* = 0.0811$ and $\Lambda/a = 2$ and 8. It can be seen that for both-type ducts, S_{gen}^* in $\Lambda/a = 2$ cases is smaller than that in $\Lambda/a = 8$ cases for all Re values. The difference of S_{gen}^* between $\Lambda/a = 2$ and $\Lambda/a = 8$ cases in half-sine ducts is much larger than that in double-sine ducts, which indicates the affects of Λ/a are more important in half-sine ducts. While evaluating the cases with fixed Λ/a, S_{gen}^* in half-sine duct with $\Lambda/a = 2$ can be seen to be smaller than that in double-sine ducts with the same Λ/a for all Re values. However, for $\Lambda/a = 8$ cases, a critical Re, equal to 1223, separates the flow situation into two regions, which is similar with that in $\Lambda/a = 4$ cases. For Re less than 1223, S_{gen}^* is smaller in half-sine ducts, but for cases with Re larger than 1223 S_{gen}^* in double-sine ducts is smaller. Accordingly, it can be concluded that for $\Lambda/a = 2$ cases, the half-sine duct is favorable for all Re values, whilst for $\Lambda/a = 4$ and 8, the favorable case is half-sine duct when Re is small, and turns to be double-sine duct for larger-Re cases. The overall evaluation of the four cases as shown in Fig. 9 exhibits clearly that the half-sine duct with $\Lambda/a = 2$ is the optimal choice since it has the minimal S_{gen}^* for all Re values.

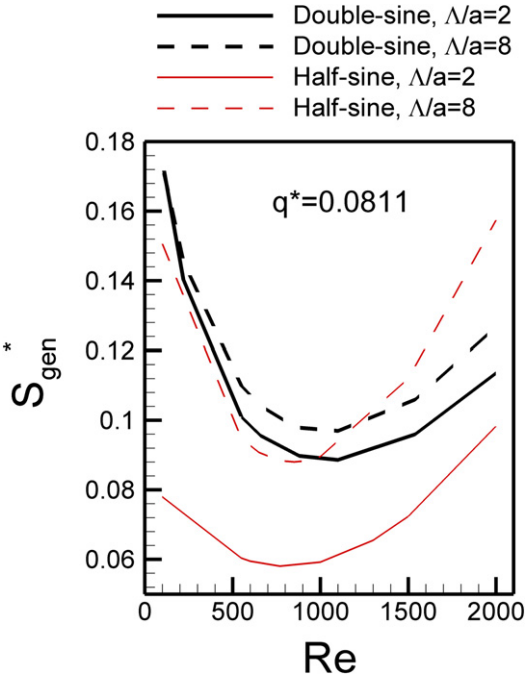

Fig. 9. Effects of Λ/a on S^*_{gen} for double- and half-sine ducts. $q^* = 0.0811$.

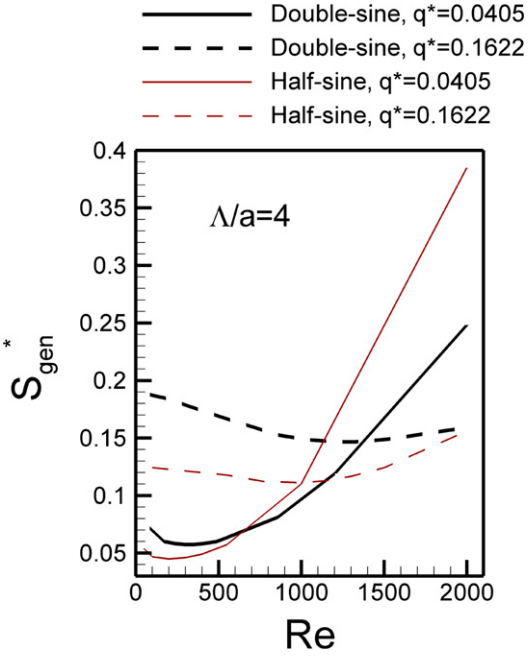

Fig. 10. Effects of q^* on S^*_{gen} for double- and half-sine ducts. $\Lambda/a = 4$.

Fig. 10 shows the relationship between S^*_{gen} and Re for the two-type ducts with $\Lambda/a = 4$, and $q^* = 0.0405$ and 0.1622, from which the influence of external heat flux is investigated. For the smaller heat flux case ($q^* = 0.0405$), S^*_{gen} in most range of Re cases considered in the current study is larger in half-sine ducts. Only for cases with Re less than 660, S^*_{gen} becomes smaller in half-sine duct. As for the larger heat flux cases ($q^* = 0.1622$), since the entropy generation is more dominated by heat transfer irreversibility due to the higher heat flux, and the double-sine ducts bear more entropy generated from heat transfer, S^*_{gen} in double-sine duct becomes larger than that in half-sine ducts for all Re cases. These results reveal the half-sine duct is favorable when q^* is larger, and the double-sine duct is favorable when q^* is smaller. Besides, it is noted the difference of S^*_{gen} magnitudes between the two ducts decreases as Re increases since the entropy generation turns to be more dominant by frictional irreversibility instead of heat transfer irreversibility as Re increases. Fig. 10 also reveals S^*_{gen} in the cases with larger q^* is not certainly larger than that in cases with smaller q^*. Only when Re is low, S^*_{gen} in larger-q^* cases is larger. This is due to that S^*_T is the dominant term in larger-q^* cases and it increases with q^*. As for larger-Re cases, the entropy generation is dominated by S^*_P. As pointed out in the previous study [17], the influence of heat flux on velocity fields is minor since the temperature raise is limited for the heat flux considered. Therefore, S'''_P, which is principally dependent on the velocity gradient, is not significantly affected by heat flux. However, due to temperature term and the normalization of $\dot{Q}/T_0$ appear in the denominators of the definitions of S'''_P and S^*_P (see Eqs. (8) and (10)), respectively, S^*_P is induced to become larger in the smaller q^* cases. Consequently, S^*_{gen} becomes larger in smaller-q^* cases when Re is larger. Based on Fig. 10, it can be seen that there exists an optimal Re to induce the minimal S^*_{gen} for all of the four cases. For half-sine ducts, the optimal Re's are 200 and 1000 for $q^* = 0.0405$ and 0.1622, respectively. For double-sine ducts, the optimal Re's are 300 and 1300 for $q^* = 0.0405$ and 0.1622, respectively.

4.6. Minimal entropy generation and optimal Re in double- and half-sine ducts

Fig. 11 presents the important information about the minimal S^*_{gen} for all cases of double- and half-sine ducts with various Re, Λ/a and q^* studied in the current paper. In the figure, the numbers noted beside the symbols of lines indicate the optimal Re to induce the minimal S^*_{gen}. From the figure, a general trend exhibits that the magnitudes of minimal S^*_{gen} increase as q^* increases, and the values of minimal S^*_{gen} in half-sine ducts are lower than those in double-sine ducts for all cases with specified Λ/a and q^*. Based on the results, the half-sine duct could be concluded as the optimal option when Λ/a and q^* are specified, and Re is left as an adjustable design parameter. Besides, it is noted that the half-sine duct with $\Lambda/a = 2$ has the minimal value of S^*_{gen} among all the cases. By using the flow configuration and Re, the least irreversibility and best exergy utilization could be achieved in the thermal system.

5. Conclusions

The developing laminar forced convection and entropy generation in both double- and half-sine ducts are investigated in the present paper with numerical methods. The studied cases cover Re ranging from 86 to 2000, aspect ratio $\Lambda/a = 2$, 4 and 8, and $q^* = 0.0405, 0.0811$ and 0.1622. Several important conclusions are as follows.

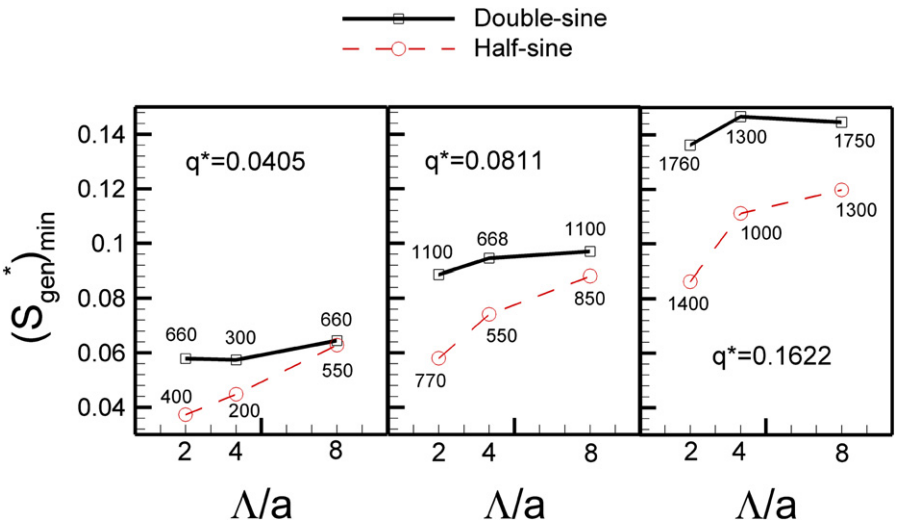

Fig. 11. The minimal S^*_{gen} and optimal Re for double- and half-sine ducts with different Λ/a.

(1) For both of double- and half-sine ducts, the higher-velocity fluids distribute in the duct central core with increasing area and magnitudes of largest velocity along the downstream. The largest W^* in half-sine ducts is 2.0, which is larger than 1.71 in double-sine ducts.

(2) The temperature rise is more serious in the half-sine duct, in which the maximum T^* is 0.15 and appears in the sharp lower corner. The maximum T^* in the double-sine duct appears in the top and lower corners, and its value is only 0.08, nearly half of the maximum T^* in the double-sine duct.

(3) In both-type ducts, Nu decreases gradually from the highest value at duct entrance toward the fully developed values. Nu in double-sine ducts is higher than that in half-sine ducts.

(4) In both-type ducts, S'''_{gen} in the duct central core is most minor, whereas the most serious entropy generation concentrates in the duct right-lower corner, which is resulted from the most serious velocity and temperature gradients in the region. The largest S'''_{gen} in half-sine duct is much larger than that in double-sine duct.

(5) For both-type ducts, the increase of Re causes the increase of S^*_P and the decrease of S^*_T simultaneously. S^*_T/S^*_{gen} is smaller in half-sine ducts for all Re cases, which indicates the flows in half-sine duct sustain more frictional irreversibility than heat transfer irreversibility.

(6) For $\Lambda/a = 2$ cases with $q^* = 0.0811$, S^*_{gen} in half-sine ducts is lower than that in double-sine ducts for all Re cases. For $\Lambda/a = 4$ cases with $q^* = 0.0811$, a critical Re exists to separate the flow situation into two regions. When Re is less than 1125, S^*_{gen} in the half-sine duct is lower than that in the double-sine duct, and accordingly half-sine duct is the favorable choice. On the contrary, the favorable choice turns to be the double-sine duct when Re is larger than 1125. The situation for $\Lambda/a = 8$ cases with $q^* = 0.0811$ are similar with $\Lambda/a = 4$ cases. The critical Re for $\Lambda/a = 8$ cases is 1223.

(7) For $\Lambda/a = 4$ cases with $q^* = 0.0405$, S^*_{gen} is smaller in half-sine duct only when Re less than 660. When q^* increases to 0.1622, S^*_{gen} in double-sine duct becomes larger than that in half-sine ducts for all Re cases. In general, for the cases with larger q^* and lower Re, the half-sine duct should be used, whereas for the cases with smaller q^* and larger Re, the double-sine duct should be used for the minimal entropy generation.

(8) A general trend shows that the magnitudes of minimal S^*_{gen} increase as q^* increases, and the values of minimal S^*_{gen} in half-sine ducts are lower than those in double-sine ducts for all cases with specified Λ/a and q^*. Among all the cases studied, the half-sine duct with $\Lambda/a = 2$ has the minimal S^*_{gen}, and thus is concluded as the optimal option for achieving the least irreversibility and best exergy utilization in the thermal system.

References

[1] R.K. Shah, W.W. Focke, Plate heat exchangers and their design theory, in: R.K. Shah, E.C. Subbarao, R.A. Mashelkar (Eds.), Heat Transfer Equipment Design, Hemisphere, Washington, DC, 1988, pp. 227–254.

[2] W.W. Focke, J. Zachariades, I. Olivier, The effect of the corrugation inclination angle on the thermohydraulic performance of plate heat exchangers, Int. J. Heat Mass Transfer 28 (8) (1985) 1469–1479.

[3] R.L. Heavner, H. Kumar, A.S. Wannizrachi, Performance of an industrial plate heat exchanger: effect of chevron angle, AIChE, Sym. Ser. 89 (295) (1993) 65–70.

[4] H. Martin, A theoretical approach to predict the performance of chevron-type plate heat exchangers, Chem. Engrg. Process. 35 (1996) 301–310.

[5] J.Y. Jang, C.N. Lin, A numerical analysis of three-dimensional heat transfer and fluid flow in chevron plate channels, ASHRAE Transactions: Symposia, MN-00-14-2, 856–863.

[6] L. Fisher, H. Martin, Friction factors for fully developed laminar flow in ducts confined by corrugated parallel walls, Int. J. Heat Mass Transfer 40 (3) (1997) 635–639.

[7] J. Ding, H. Manglik, Analytical solutions for laminar fully developed flows in double-sine shaped ducts, Heat Mass Transfer 31 (1996) 267–277.

[8] R.M. Manglik, J. Ding, Laminar flow heat transfer to viscous power-law fluids in double-sine ducts, Int. J. Heat Mass Transfer 40 (6) (1997) 1379–1390.

[9] A. Bejan, Entropy Generation Minimization, CRC Press, Boca Raton, FL, 1996.
[10] A. Bejan, Entropy Generation Through Heat and Fluid Flow, Wiley, New York, 1982.
[11] P.K. Nag, K. Naresh, Second law optimization of convection heat transfer through a duct with constant heat flux, Int. J. Energy Res. 13 (1989) 537–543.
[12] A.Z. Sahin, Irreversibilities in various duct geometries with constant wall heat flux and laminar flow, Energy 23 (6) (1998) 465–473.
[13] A.Z. Sahin, Thermodynamics of laminar viscous flow through a duct subjected to constant heat flux, Energy 21 (12) (1996) 1179–1187.
[14] S.Z. Shuja, Optimal fin geometry based on exergoeconomic analysis for a pin-fin array with application to electronics cooling, Exergy 2 (2002) 248–258.
[15] T.H. Ko, K. Ting, Entropy generation and thermodynamic optimization of fully developed laminar convection in a helical coil, Int. Commun. Heat Mass Transfer 32 (2005) 214–223.
[16] T.H. Ko, K. Ting, Entropy generation and optimal analysis for laminar forced convection in curved rectangular ducts: A numerical study, Int. J. Thermal Sci. 45 (2) (2006) 138–150.
[17] T.H. Ko, Numerical investigation on laminar forced convection and entropy generation in a curved rectangular duct with longitudinal ribs mounted on heated wall, Int. J. Thermal Sci. 45 (4) (2006) 390–404.
[18] T.H. Ko, K. Ting, Optimal Reynolds number for the fully developed laminar forced convection in a helical coiled tube, Energy 31 (12) (2006) 1806–1816.
[19] T.H. Ko, Thermodynamic analysis of optimal curvature ratio for fully developed laminar forced convection in a helical coiled tube with uniform heat flux, Int. J. Thermal Sci. 45 (7) (2006) 729–737.
[20] T.H. Ko, Numerical investigation on laminar forced convection and entropy generation in a helical coil with constant wall heat flux, Numer. Heat Transfer, Part A 49 (3) (2006) 257–278.
[21] T.H. Ko, Analysis of optimal Reynolds number for developing laminar forced convection in double-sine ducts based on entropy generation minimization principle, Energy Conversion and Management 47 (2006) 655–670.
[22] T.H. Ko, Numerical analysis of entropy generation and optimal Reynolds number for developing laminar forced convection in double-sine ducts with various aspect ratios, Int. J. Heat Mass Transfer 49 (3–4) (2006) 718–726.
[23] B.E. Launder, D.B. Spalding, The numerical computation of turbulent flows, Computer Methods Appl. Mech. Engrg. 3 (1974) 269–289.
[24] S.V. Patankar, Numerical Heat Transfer and Fluid Flow, Hemisphere, Washington, DC, 1980.
[25] CFD RC, ESI-CFD Inc., ESI Group, Huntsville, AL, USA.